Rheol Acta (2011) 50:717–728
DOI 10.1007/s00397-010-0527-9

ORIGINAL CONTRIBUTION

Scaling behavior of the elastic properties of non-dilute MWCNT–epoxy suspensions

Fatemeh Khalkhal · Pierre J. Carreau

Received: 9 October 2010 / Revised: 14 December 2010 / Accepted: 23 December 2010 / Published online: 13 April 2011

Abstract In this paper, the network structure of multi-walled carbon nanotube (MWCNT)–epoxy suspensions was investigated under the influence of flow history and temperature using the scaling behavior of the linear viscoelastic properties of the concentrated suspensions above their gel point. It is shown that the suspensions have a self-similar fractal structure with the dimension of about 2.15, characteristic of weakly flocculating suspensions and their elasticity originates from inter- and intra-floc links of nanotubes. From the scaling behavior of the flow-induced storage modulus and the critical strain for the limit of linearity, it is shown that the fractal dimension and so the superstructure of the network did not change significantly under the influence of the flow history due to the initial compact structure of the network before pre-shearing. The time–temperature superposition principle was verified for the CNT suspensions and the shift factor was accounted for by an Arrhenius equation. The reduced storage and loss moduli of the suspensions using the complex modulus of the neat epoxy were shown to increase with temperature revealing more inter-particle interactions as the temperature was raised. However, it was impossible to conclude on the changes of the fractal dimensions with temperature.

F. Khalkhal · P. J. Carreau (✉)
Center for Applied Research on Polymers and Composites (CREPEC), Chemical Engineering Department, Ecole Polytechnique of Montreal, C.P. 6079 Suc. Centre-Ville, Montreal, QC H3C 3A7, Canada
e-mail: pcarreau@polymtl.ca, pierre.carreau@polymtl.ca

Keywords Carbon nanotube · Rheology · Microstructure · Scaling theory · Flow history · Fractal dimension

Introduction

Carbon nanotubes (CNTs) show many potential applications since their discovery and have been widely used to reinforce polymers and improve their physical properties, such as electrical conductivity. To control the processing and the final properties of the resulting nanocomposites, a great deal of research effort has been devoted to develop structure–property relationships.

Previous studies of the structure in dilute CNT suspensions have focused on the orientation dynamics of nanotubes under flow by employing a variety of light scattering techniques (Hobbie et al. 2003a, b; Pujari et al. 2009). Fry et al. (2005, 2006) established a quantitative relationship between the anisotropy of sheared CNT suspension structure and nanotube concentration and aspect ratio, shear rate, and the viscosity of the suspending medium. The state of flocculation (at low shear rates) and de-flocculation (at high shear rates) of CNT suspensions under flow have been probed by rheo-optical techniques by Hobbie and Fry (2006) and Lin-Gibson et al. (2004). Their investigations resulted in a universal non-equilibrium phase diagram describing a transition from solid-like networks to flowing nematics under an applied shear stress. Although very helpful information can be obtained from light scattering, they are mainly limited to dilute suspensions whereas the conductive composites are usually prepared at concentrations about the percolation threshold or even higher. In addition, in some cases, the rheological properties

originate from length scales different from the ones characterized by the light scattering; consequently, no significant change can be observed by light scattering while rheological properties show a considerable variation (for example see the work of Rahatekar et al. (2006)). On the contrary, rheology can be used to characterize the microstructure of suspensions over a wide range of concentrations.

Using rheological measurements, Wu et al. (2009) has recently developed a relationship between the aspect ratio of carbon nanotubes and the formation of a percolated network in polylactide–CNT composites. Fan and Advani (2007), Huang et al. (2006), and Song and Youn (2005) investigated the effect of the dispersion state of CNTs in different polymer matrices on the rheology of the nano-composites. We have recently (Khalkhal et al. 2011) shown that the linear viscoelastic properties of CNT–epoxy suspensions are strongly influenced by the effect of the flow history and the rate of the structure build-up after cessation of pre-shearing was quantified and its dependency on the rate of the pre-shear, the concentration, and the temperature was investigated.

On the other hand, using models based on scaling theories (Shih et al. 1990; Wu and Morbidelli 2001) and fractal theories (Potanin 1991, 1993), some in depth information about the network structure of colloidal suspensions and their evolution under flow can be obtained. Using scaling theories, the origin of the elastic behavior of the gels can be identified and the extent of their compactness can be quantified. Fractal theories can provide helpful information about the rigidness of the aggregates as well as the mechanisms of aggregate deformation and break up under flow.

In this paper, the network structure of multiwalled carbon nanotube (MWCNT)–epoxy suspensions is investigated under the influence of flow history and temperature using the scaling behavior of the linear viscoelastic properties of concentrated suspensions above their gel point. Scaling of the steady shear results with the low angular frequency storage modulus of gels resulted in formation of a master curve. Based on fractal theory, it can be assumed that a self-similar fractal network structure is present in the gels. The fractal network dimension (without pre-shearing) is approximated to be 2.15, characteristic of weakly flocculating suspensions. From scaling of linear viscoelastic (LVE) properties, it is shown that the inter- and intra-floc links of nanotubes contribute to the elasticity of the suspensions. The effect of pre-shearing and temperature on the variation of the fractal dimension is analyzed. This is helpful for describing the rheological properties of highly concentrated CNT suspensions, for which simulations based on fractal theories are impossible.

The article is organized as follows. A background review about the scaling and fractal theories is given in "Theoretical background". In "Materials and their characterization" section, details of experimental techniques and material characterization are described. The results of the rheological measurements and their relation to the scaling and fractal theories are given in "Results and discussion". In "Conclusion" the important findings of the article are highlighted.

Theoretical background

Scaling theory

Shih et al. (1990) developed a scaling theory for colloidal gels similar to the one for semi-dilute polymeric solutions developed by de Gennes (1979). It was assumed that the network structure of the gel is constituted of closely packed clusters with the fractal dimension d_f, which depends on the aggregation mechanism. For fast aggregation, where flocs grow by merging into one another as soon as they collide, $d_f = 1.7$–1.8 similar to the one for cluster–cluster aggregation and $d_f = 2.0$–2.2 for slow aggregation or the so-called reaction-limited aggregation, where flocs penetrate to one another partially after collision (Larson 1999). The scaling relation between the average floc size ξ and the particle concentration ϕ, provided that the internal concentration of particles ϕ_{int} can be approximated by the overall particle concentration ϕ, is given by

$$\xi \sim \phi^{\frac{1}{(d_f - d)}}, \tag{1}$$

where d is the Euclidean dimension. According to this theory, the elastic properties of flocs are dominated by their effective backbone of size ξ, where the elastic backbone was approximated to be a linear chain of springs (with a radius of gyration ξ), assuming that the aggregates have few loops. Thus, the elastic constant of a floc K_ξ with size ξ can be approximated by

$$K_\xi \sim \frac{K_0}{\xi^{x+2}}, \tag{2}$$

where K_0 is the bending constant between two neighboring springs and x is the fractal dimension of clusters, which is in the range of 1 and d_f ($1 < x < d_f$). Consequently, the macroscopic elastic constant of a system

with the size L can be written in terms of that of the individual flocs as

$$G' \sim \left[\frac{L}{\xi}\right]^{d-2} K_\xi. \tag{3}$$

According to Shih et al. (1990), the macroscopic elasticity originates whether from intra-floc links (strong-link region) or from the inter-floc links between the particles (weak-link region). The drawback of this model is that, in some cases, it fails by predicting a negative value for the fractal dimension x of clusters. On the other hand, Wu and Morbidelli (2001) defined a macroscopic elasticity by the contributions from inter- and intra-floc links. As a result, K_ξ in Eq. 3 should be replaced by K_{eff} given by

$$\frac{1}{K_{\text{eff}}} = \frac{1}{K_\xi} + \frac{1}{K_l}, \tag{4}$$

where K_ξ is the intra-floc elastic constant and K_l is the inter-floc elastic constant and it is independent of the microstructure parameters of the flocs. By approximating $1/\left(1 + K_\xi/K_l\right)$ with $\left(K_l/K_\xi\right)^\alpha$ where $\alpha \in [0, 1]$ and substituting this correlation into Eqs. 3 and 1, the final correlation for the macroscopic elasticity with particle concentration can be obtained as

$$G' \sim \phi^{\frac{\beta}{d-d_f}}, \tag{5}$$

where

$$\beta = (d-2) + (x+2)(1-\alpha). \tag{6}$$

Similarly, the critical strain for the maximum limit of linearity was approximated by

$$\gamma_c \sim \phi^{-n} \sim \phi^{\frac{d-\beta-1}{d-d_f}}. \tag{7}$$

For $\alpha = 0$, the correlations 5 and 7 reduce to that of Shih et al. (1990) for the strong-link region and for $\alpha = 1$, they lead to the ones for weak-link region. By relating the yield stress to the elastic modulus as $\tau_y = G'\gamma_c$, one obtains:

$$\tau_y \sim \phi^{\frac{d-1}{d-d_f}}. \tag{8}$$

Fractal theory

Buscall et al. (1987) and Chen and Russel (1991) studied the rheological behavior of strongly flocculated suspensions and showed that the suspension yield stresses and moduli had a power-law dependence on particle concentration supporting the idea that the networks of the flocculated suspensions have a heterogeneous structure consisting of interconnected fractal aggregates. Potanin (1993) performed computer simulations of the deformation and breakup of colloidal aggregates under shear flow and classified the aggregates into rigid and soft. Rigid aggregates elastically respond to small deformations. This elastic response is characterized by an elastic modulus and a yield stress that are related to each other and are correlated to the radius of gyration (ξ) as well as the internal concentration (ϕ_{int}) by a power-law given by

$$G' \sim \tau_y \propto \xi^{-\gamma} \propto \phi_{\text{int}}^{\gamma_1}, \tag{9}$$

where from Eq. 1 $\phi_{\text{int}} \sim \xi^{(df-d)}$ and thus γ_1, the power-law exponent relating the storage modulus to the concentration is

$$\gamma_1 = \gamma/\left(3 - d_f\right), \tag{10}$$

where d equals 3. In rigid aggregates, the interaction potential of particles is non-central and is described through a function of angles between neighboring bonds. On the other hand, the interaction potential of particles is purely central in soft aggregates and depends on the distance between the centers of the neighboring particles. In addition, the internal structure of the soft aggregates does not respond elastically to small deformations. Sonntag and Russel (1986, 1987) showed that the radius of gyration of aggregates decrease with shear rate in a power-law manner,

$$\xi \sim \dot{\gamma}^{-m}. \tag{11}$$

Equating $\eta\dot{\gamma}$ to τ_y, for the rigid aggregates, yields

$$m = m_{\text{rigid}} = 1/\gamma. \tag{12}$$

Furthermore, comparing Eqs. 5 with 9 and 10, one can conclude that $m_{\text{rigid}} = 1/\beta$. For purely rigid aggregates, m_{rigid} is estimated to be in the range of 0.23–0.29 and for purely soft aggregates, m_{soft} is a value about 0.4–0.5 (Potanin 1993). It should be noted that these values for m_{rigid} and m_{soft} should be considered as lower and upper bounds of m; thus, for a typical colloidal suspension, the expected value of m is in the range of [0.23, 0.5].

Materials and their characterization

An epoxy Epon 828 (HEXION Speciality Chemicals Inc.) with a density of 1.16 g/mL and viscosity of 12.33 Pa s (at 25°C) was used as the dispersing medium and suspensions of nanotube–epoxy were prepared by mixing in an EXAKT three roll mill (from EXAKT Technologies, Inc.) at room temperature. Multiwall carbon nanotubes from Cheap Tubes Inc.© were initially characterized by transmission electron microscopy. The

details of CNT characterization is described in a previous article (Khalkhal et al. 2011). The nanotubes were as long as 0.1–2.2 μm with the average aspect ratio of 45. They were shown to be rigid in the range of the shear rates studied (the effective stiffness of the nanotubes ranges from $S^{\text{eff}} \approx 0.385$ to 3850 when $\dot{\gamma} = 0.01 - 100\,\text{s}^{-1}$ where $S^{\text{eff}} = E_Y \pi d^4 / \left(64\eta_s \dot{\gamma} L^4\right)$ according to Switzer and Klingenberg (2003). E_Y (~40 GPa according to Hobbie and Fry (2007)) is the Young modulus of the nanotubes, d (14.86 nm) and L(670 nm) are mean values of the outer diameter and length of the nanotubes, η_s is the viscosity of the suspending medium (12.33 Pa s for the neat epoxy at room temperature) and $\dot{\gamma}$ is the shear rate. The effective stiffness of the MWCNTs is large enough to categorize them among rigid rods).

Samples of CNT–epoxy suspensions were prepared at different concentrations and the details of the mixing process by a three roll mill and sample preparation are presented in a previous article (Khalkhal et al. 2011). A Physica MCR501 (Anton Paar) rheometer with a parallel plate geometry (PP50 with the diameter of 49.959 mm) and 1 mm gap was used to perform the rheological measurements at 25°C. Temperature was controlled by a Peltier (P-PTD 200) system. Steady shear viscosity measurements were performed at different gaps (0.8, 1, and 1.2 mm) to prove the absence of wall slip effects during the experiments. The reproducibility of the measurements was verified by repeating the experiments several times. The maximum error was calculated to be about ±15%.

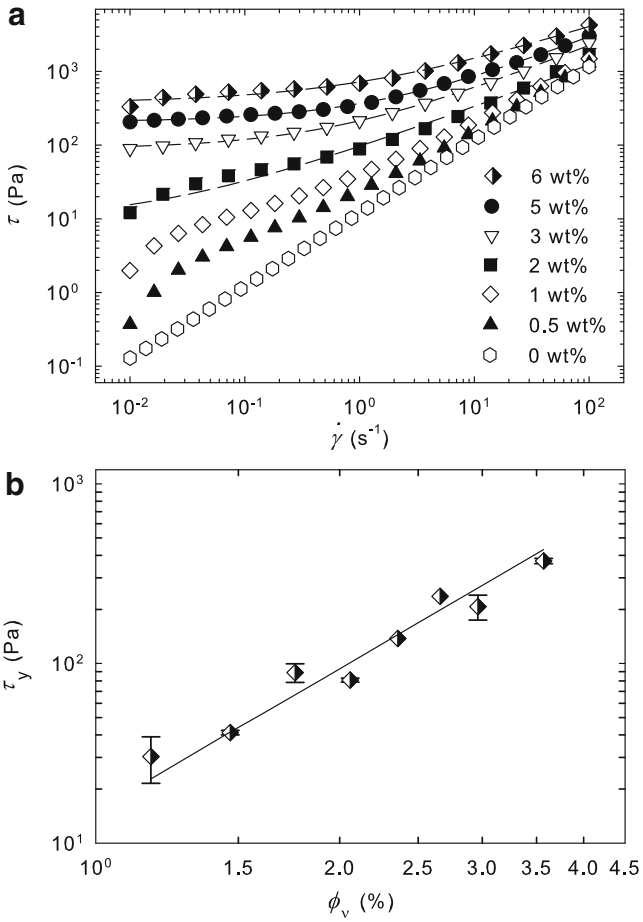

Fig. 1 **a** Steady-shear measurement of MWCNT suspensions at different concentrations. The *lines* show the best fits of the data using the Herschel–Bulkley model where the apparent yield stress appears. **b** Scaling behavior of the apparent yield stress obtained using the Herschel–Bulkley model with volume concentration of MWCNTs. The *line* shows the best power-law fit

Results and discussion

Initially, a set of frequency sweep measurements were performed to determine linear viscoelastic properties of the suspensions. We observed that the suspensions of 0.5 and 1 wt.% exhibited a liquid-like behavior similar to the neat epoxy and the loss modulus was larger than the storage modulus. At 2 wt.%, the storage and loss moduli showed a transition from liquid-like to solid-like behavior at low angular frequencies, which is an indication of the formation of a percolated CNT network. At the critical concentration of about 2 wt.% and above, the elastic modulus of the suspensions was significantly larger than the viscous one. Consequently, 2 wt.% was considered as the rheological percolation threshold. The formation of a percolated network was confirmed by the emergence of an apparent yield stress at about 2 wt.% and higher concentration. Figure 1a shows the steady shear measurements performed from the low shear of 0.01 s^{-1} to high shear of 100 s^{-1} for a range of concentrations. The results presented in this figure were confirmed to overlap by the steady shear measurement in reverse direction.

The apparent yield stress was estimated from curve fitting using the Herschel–Bulkley model that yields:

$$\tau = \tau_y + a\dot{\gamma}^b, \tag{13}$$

where τ_y is the apparent yield stress, a is the consistency index, and b is the flow behavior index. The lines in Fig. 1a show the best fit of the experimental results with the Herschel–Bulkley model. For concentrations lower than 2 wt.%, the curve fitting did not converge. Moreover, the apparent yield stress scales with the volume concentration of the suspensions as shown in Fig. 1b. More samples with different concentrations in the range

of 2 to 6 wt.% were prepared to obtain additional apparent yield stress values and a better power-law fit. The line represents the best power-law fit of the apparent yield stress, which scales with concentration as $\tau_y \sim \phi_v^{2.64\pm0.16}$ $\left(R^2 = 0.973\right)$.

Scaling behavior of steady-shear results

Using the low frequency storage modulus of gels, Chow and Zukoski (1995) (frequencies in the range of 0.001 to 10 Hz) and Fagan and Zukoski (1997) (at frequency of 1 Hz) showed that a master curve of the steady-shear measurements can be obtained that was weakly dependent on the particle volume fraction, particle size, particle size distribution, or the surface potential. To obtain the master curve, the steady-shear stress (τ) should be scaled with the low angular frequency storage modulus of the gels, G'_0, and the shear rate, $\dot{\gamma}$, with η_s/G'_0, where η_s is the viscosity of the suspending medium and η_s/G'_0 is the characteristic time of the suspension. Figure 2 shows the steady-shear results scale with the low angular frequency (1 rad/s) storage modulus of the CNT suspensions at 2 wt.% and higher concentrations. From this figure, it is clear that the results are weakly dependent on concentration. This weak dependence suggests that the network structure of the suspensions is self-similar above the percolation threshold and is constituted of closely packed clusters (flocs) that have a fractal nature.

In the following sub-sections, the fractal structure of the suspensions is analyzed more quantitatively and the effect of flow history and temperature are investigated.

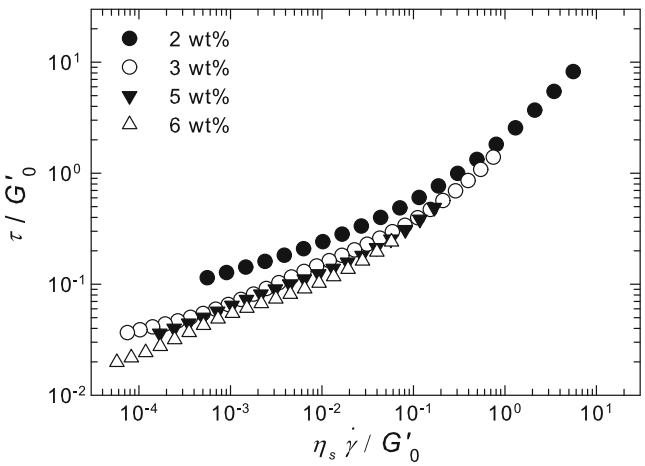

Fig. 2 Scaling behavior of steady shear data with low angular frequency (1 rad/s) storage modulus of the suspensions

Scaling behavior of linear viscoelastic properties

We assume that the aggregates were initially rigid, so their behavior can be characterized by the storage modulus and yield stress that scale with the concentration of particles. The maximum strain for the limit of linearity, γ_c, was considered as the strain above which $G'/G'_0 < 0.9$, where G'_0 is the plateau storage modulus in the linear region. The scaling behavior of γ_c as well as the storage modulus (before pre-shearing) at the low angular frequency of 1 rad/s $\left(G'_0\right)$ with the volume concentration was verified above the gel point of 1.17 vol.% (2 wt.%) as shown in Fig. 3. The scaling behavior of the elastic properties of the suspensions with concentration supports the fact that the suspensions have a space-filling network, i.e., they are formed by individual aggregates (clusters) growing into one another and filling the space. The experimental data were fitted with power-law correlations and the best fits are shown as dashed lines in Fig. 3. From Fig. 3a, the storage

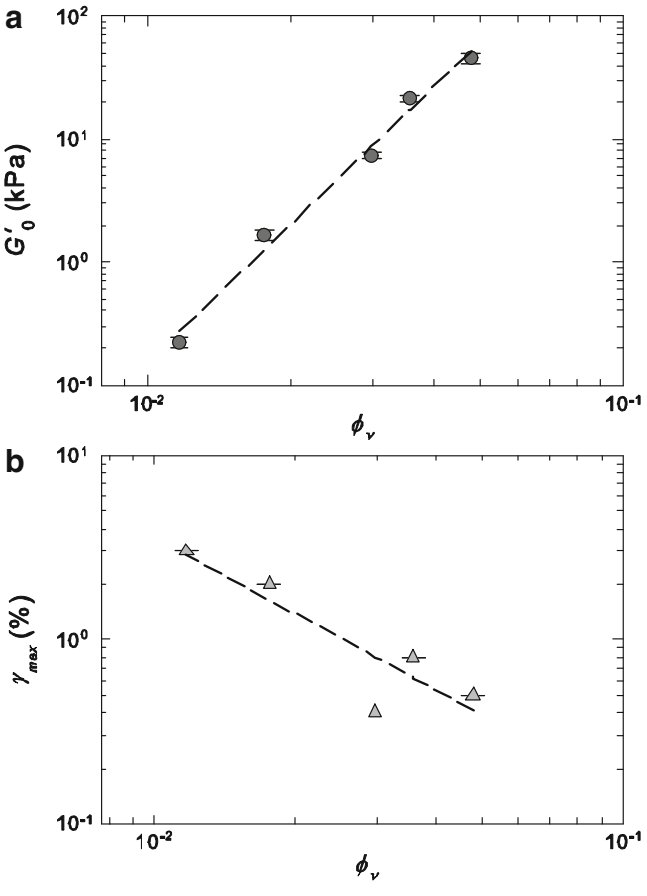

Fig. 3 Scaling behavior of **a** the elastic modulus and **b** the critical strain before pre-shearing as a function of volume concentration of MWCNTs

modulus scales with concentration as $G_0' \sim \phi_v^{\gamma_1}$, where γ_1 is equal to 3.74 ($R^2 = 0.988$) and from Fig. 3b, $\gamma_c \sim \phi_v^{-n}$, where n is equal to 1.378 ($R^2 = 0.795$). Using Eqs. 5–7, the fractal dimension d_f was estimated to be 2.15, revealing that the network structure of CNT suspensions is among the slowly flocculating suspensions (Larson 1999). A very similar value of d_f was calculated using Eq. 8 with $\tau_y \sim \phi_v^{2.64\pm0.16}$. Hobbie and Fry (2006, 2007) reported a fractal dimension of 2.45 for MWCNTs dispersed in low-molecular-mass polyisobutylene showing the presence of a slightly denser network structure than our CNT suspensions. The slightly larger value could be due to more entanglements of longer nanotubes used in their study ($L \sim 10$ μm, with $L/d \sim 200$) compared to the short nanotubes used in this study ($L \sim$ 0.1–2.2 μm, with $< L/d > \sim 45$). On the other hand, Chatterjee and Krishnamoorti (2007) reported a fractal dimension of 2.1 ± 0.3 for single-walled carbon nanotubes (SWCNTs) with an effective $L/d \sim 650$ dispersed in polyethylene oxide (PEO), which is similar to the value obtained for our MWCNT suspensions.

From Fig. 3b, γ_c decreases as the volume concentration increases. This means that although the inter-particle interactions increase with concentration and a stronger network forms, the structure becomes more fragile as the concentration increases. In the case of SWCNTs in PEO, Chatterjee and Krishnamoorti (2007) observed a similar decrease in γ_c with concentration. Using the Shih et al. (1990) theory, they reported that the suspension elasticity originates mainly from short-range interactions between carbon nanotubes and the multiple connections in the percolating network. However, using the scaling theory of Shih et al. (1990), the fractal backbone dimension x was calculated to be negative in our case, which does not have a physical meaning. On the other hand, Wu and Morbidelli (2001) introduced the parameter α that was calculated from Eq. 6 to be about 0.3–0.4 when the fractal backbone dimension x is in the range of 1.0–1.3, revealing the fact that in CNT suspensions used here the elasticity of the network is a contribution of the inter- and intra-floc links between nanotubes. Moreover, from Eqs. 5 and 7, β was calculated to be 3.17 from which m equals 0.32. This value is in the range of $m_{\text{rigid}} \sim 0.23 - 0.29$ and $m_{\text{soft}} \sim 0.4 - 0.5$ reported by Potanin (1993) using computer simulations. It is very similar to the experimental value of 0.35 reported by Sonntag and Russel (1986, 1987) for polystyrene lattices. Mobuchon et al. (2009) obtained different values of 0.22 and 0.42 for non-polar and polar nano-clay model suspensions, respectively. This stresses that the aggregates in the CNT network are partly rigid and partly soft and so the interaction potential of the particles is a combination of central (which depends on the distance between the centers of the neighboring particles) and non-central (which depends on angles between the adjacent bonds) components (Potanin 1993).

The evolution of the structure of colloidal suspensions under flow has been described by fractal theories (Potanin 1991, 1993; Potanin et al. 1995) from which the deformation and break up of aggregates can be modeled. However, due to high computational cost, these models are restricted to a very limited number of particles, which means that only the behavior of dilute systems can be modeled. As a result of this drawback, it is impossible to compare the rheological behavior of our CNT suspensions above their gel point using these simulation models.

The effect of flow history

In order to investigate the variation of the network structure of the suspensions under flow, the samples were pre-sheared at different rates until steady-state was reached, followed by a low angular frequency small amplitude oscillatory shear at very small deformations in the linear viscoelastic region (0.0118, 0.01, 0.0025, and 0.00174 for 0.5, 1, 5, and 6 wt.%, respectively, and 0.0072 for 2 and 3 wt.%) for sufficient time (5,000 s) to approach a quasi-equilibrium state. From the scaling behavior of the linear viscoelastic properties of the pre-sheared suspensions, the fractal dimension was estimated using the scaling theories and its variation with the pre-shear rate is explained in the light of the fractal theories.

The variation of the limit for the linear viscoelastic region with flow history was initially verified. The effect of the pre-shear rate was analyzed on the strain sweep results of the suspensions at different concentrations and pre-shear rates, followed by 5,000 s rest to ensure the results were not affected by a fast structural evolution right after pre-shearing. Figure 4 presents the results for the strain sweep of a 3 wt.% suspension pre-sheared at 1 and 100 s^{-1} carried out at 0.1 and 10 rad/s, respectively. The y-axis data of the pre-sheared suspension at 1 s^{-1} was multiplied by a factor 5 for a better representation.

From this figure, γ_c for the 3 wt.% suspension is shown to increase from 1.27% to 2% when the pre-shear rate, $\dot{\gamma}_i$, increases from 1 to 100 s^{-1}. This means the structure is more fragile after pre-shearing at lower rate of 1 s^{-1}. A similar result was obtained at other concentrations. However, the effect of pre-shearing on γ_c was more significant at lower concentrations. These results will be used shortly to scale γ_c with concentration

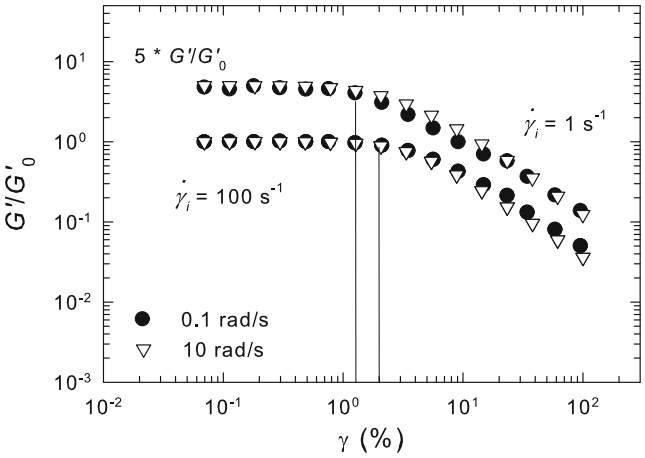

Fig. 4 Strain sweep of reduced elastic modulus carried out at 0.1 and 10 rad/s after pre-shear rates of 1 and 100 s^{-1} for a 3 wt.% MWCNT suspension in epoxy (G'_0 is the storage modulus of the linear zone)

via power-law correlations and to estimate the variation of d_f with pre-shear rate.

The effect of pre-shearing on the small amplitude oscillatory shear (SAOS) data at 1 rad/s and strain amplitude of 0.0072 for the 3 wt.% suspension is shown in Fig. 5. The solid lines show the best exponential fits of the experimental data with the following correlation from Khalkhal et al. (2011).

$$G'(t) = G'_i + \left(G'_\infty - G'_i\right)\left[1 - \exp\left(-t/\tau\right)\right], \qquad (14)$$

where G'_i and G'_∞ are the storage modulus right after pre-shearing (at $t = 0$) and 5,000 s after cessation of pre-shearing, respectively, and τ is a characteristic time. Some data have been eliminated to clarify the curves. For the sake of brevity, the structure build-up curves for other concentrations are not presented, but have been used for further analysis. More details about the effect of the flow history can be found in Khalkhal et al. (2011).

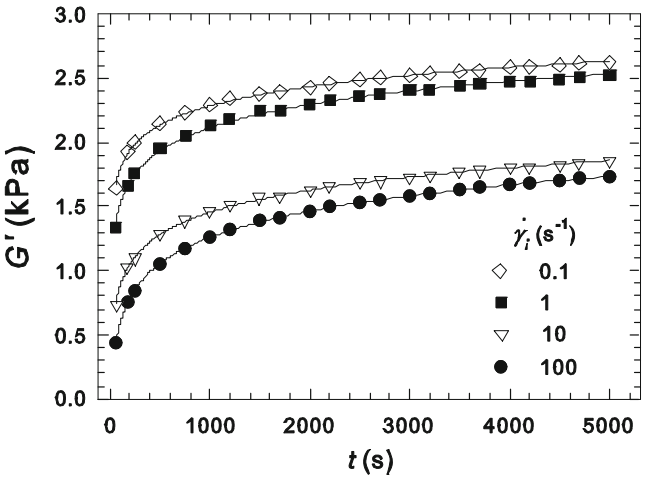

Fig. 5 Increases of the elastic modulus for 3 wt.% MWCNT–epoxy suspensions with time after cessation of shear flow for different pre-shear rates. The SAOS measurements were carried out at 1 rad/s and at a strain amplitude of 0.0072

This figure reveals that the suspension storage modulus evolves after cessation of shear flow. The elastic modulus of the 3 wt.% suspension strongly depends on the rate of the pre-shear and it increases as the rate of the applied pre-shear decreases. Moreover, the storage modulus and so the suspension structure build up very fast shortly after cessation of pre-shearing and then more slowly to reach an equilibrium value at 5,000 s or longer. In a previous article (Khalkhal et al. 2011), it has been shown that pre-shearing at low rates results in the formation of a denser structure and more entanglements between nanotubes while pre-shearing at high rates break down some interconnections between nanotubes and their clusters. This results in the formation of an interconnected network at lower concentrations when suspensions are pre-sheared at low rates while the percolation threshold shifts to higher concentrations by pre-shearing at high rates. Figure 5 shows a similar effect on the structure where pre-shearing at lower rates of 0.1 and 1 s^{-1} resulted in more entanglements and higher elastic modulus. However, by increasing the rate of pre-shear to 10 s^{-1}, some interconnections between clusters and nanotubes broke down at the expense of lower elasticity of the suspension.

The storage modulus at equilibrium (i.e., 5,000 s) is denoted by G'_∞, which is a function of concentration and pre-shear rate as shown in Fig. 6. The dashed lines are the best power-law fits of G'_∞ with the pre-shear rate that yields:

$$G'_\infty = \kappa\, \dot{\gamma}_i^{-\varepsilon}, \qquad (15)$$

where κ and ε are constants that depend on concentration.

The error for the best fit was calculated using the normalized standard deviation that can be defined as $\sigma_N = \sqrt{\frac{\sum\left\{\left[(G'_\infty)_{exp} - (G'_\infty)_{model}\right]/(G'_\infty)_{exp}\right\}^2}{N}}$ (where N is number of experimental data) and is a more suitable parameter in this case than R^2 to estimate the error correctly. It is worth to note that ε varies from 0.365 at 0.5 wt.% (with $\sigma_N = 0.358$) to 0.003 at 6 wt.% (with $\sigma_N = 0.035$). Hence, the dependence of G'_∞ on the flow history becomes less pronounced by increasing concentration.

Considering Eq. 15, the storage modulus can be interpolated at other pre-shear rates in the range of 0.01

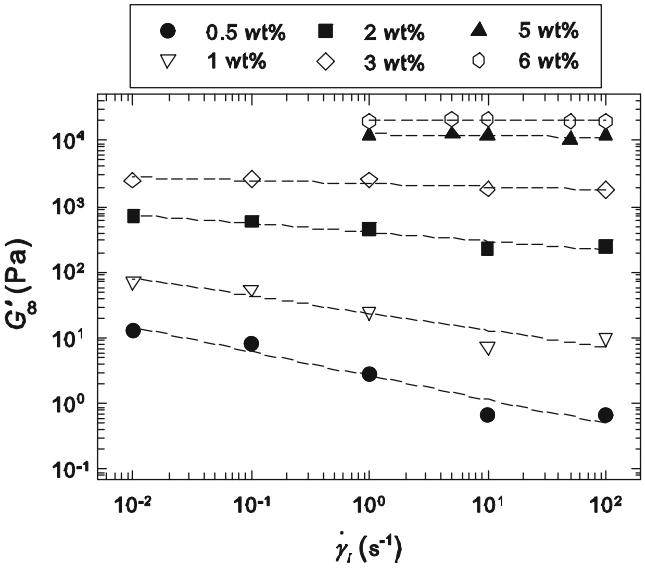

Fig. 6 Dependence of the storage modulus on pre-shear rate for the pre-sheared MWCNT suspensions followed by 5,000 s rest (G'_∞). SAOS measurements were carried out at 1 rad/s in the linear region

to 100 s^{-1} having ε and κ from curve fitting; this is how $(G'_\infty)_{\text{model}}$ was calculated. The steady-shear results can be rescaled using $(G'_\infty)_{\text{model}}$ instead of (G'_0) similarly as done for Fig. 2. The results reported in Fig. 7 show a master curve of the steady-shear results that is almost independent on the concentration over a wider range of concentrations compared to Fig. 2, from 0.5 to 6 wt.%. Note that the only large departures from the master curve are observed for the low concentration suspensions at the lowest shear rates. This reveals that G'_∞ can predict most of the structural changes and hence is a suitable parameter for characterizing the structure of MWCNT suspensions. However, to quantify the fractal structure of the suspensions and to verify its variation under the influence of flow history (and temperature), the scaling behavior of the LVE properties of the suspensions is considered for concentrations above the percolation threshold only.

The scaling behavior of G'_∞ and the critical strain for the limit of linearity, γ_c, with the volume concentration is now verified. It should be noted that the variation of G'_∞ with the pre-shear rate, $\dot{\gamma}_i$, results in a variation of the percolation threshold with pre-shearing from near 1 wt.% at 0.1 s^{-1} to 2.5 wt.% at 100 s^{-1} as mentioned previously (Khalkhal et al. 2011). As a result, to estimate the fractal dimension correctly, the scaling behavior of the pre-sheared suspensions was verified just above the percolation threshold for each pre-shear rate. Figure 8 presents the variations of G'_∞ and γ_c with volume concentration of MWCNTs. The lines show the

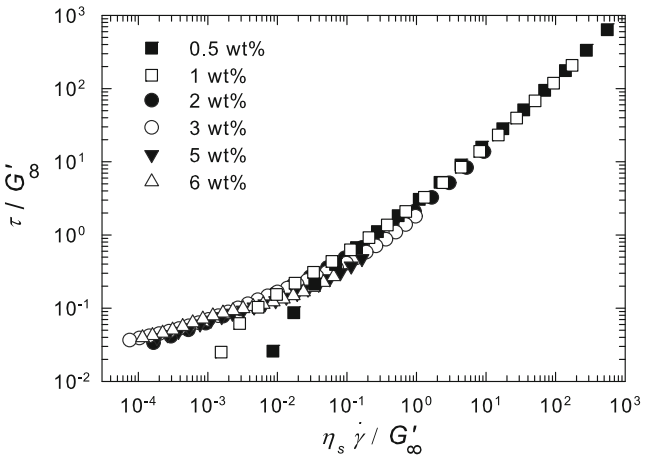

Fig. 7 Scaling behavior of steady-shear data with the low angular frequency storage modulus of the pre-sheared suspensions (G'_∞) obtained from interpolation using Eq. 15

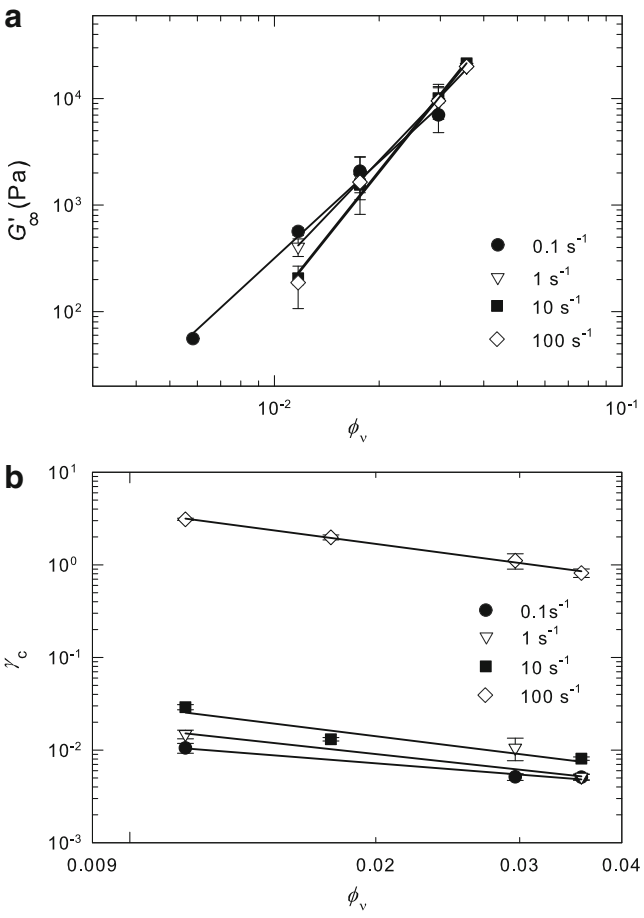

Fig. 8 Scaling behavior of **a** the elastic modulus and **b** the critical strain after pre-shearing at different rates followed by 5,000 s rest as a function of volume concentration of MWCNTs

best power-law fits with the experimental data. From Fig. 8a, the slope is shown to increase gradually with increasing pre-shear rate revealing a stronger dependence of G'_∞ on the flow history. However, as seen from Fig. 8b, the slope of γ_c with volume concentration does not change significantly, but the absolute value of γ_c increases drastically with pre-shearing. The power-law exponents from the best fits are summarized in Table 1, where $G'_\infty \sim \phi_v^{\gamma_1}$ and $\gamma_c \sim \phi_v^{-n}$. The estimated R^2 values are in the range of 0.989 to 0.998 for γ_1 and 0.916 to 0.997 for n.

From this table, it can be observed that the exponents γ_1 and n increase with pre-shear rate revealing a much stronger dependence of G'_∞ and γ_c to the volume concentration as the pre-shear rate is increased. From Eqs. 5–7 the fractal dimension can be determined and the values are also reported in Table 1. Although the exponents γ_1 and n significantly increase with pre-shear rate, the fractal dimension, d_f, increases only slightly from 2.13 at 0.1 to 2.31 at 100 s^{-1} pre-shear rates. A similar increase in the fractal dimension of a colloidal suspension was reported by Potanin (1993) and Potanin et al. (1995) that was related to the breakdown of the primary aggregates and the formation of secondary aggregates that contract as the pre-shear rate increase and form a more compact structure with larger d_f. However, for initially dense aggregates with $d_f > 2.0$, the extent of the increase in the d_f was not very significant, which is the case for the CNT suspensions used here with an initial d_f of about 2.15. Our results reveal that although the suspensions structure is sensitive to the flow history, the superstructure of the network is not influenced considerably and the variation of d_f with pre-shear rate remains within the experimental error. Consequently, one should consider the fractal dimension of the pre-sheared suspensions to be in the range of 2.13 ± 0.14 to 2.31 ± 0.15.

The power-law exponent for the variation of the radius of gyration of aggregates (ξ) with the shear rate under the influence of flow history, m, was also determined for the suspensions to be in the range of 0.36–0.38 and in the limit between m_{rigid} and m_{soft}, clarifying the importance of both central and non-central components of the interaction potential of particles in the pre-sheared suspensions. In addition, considering a typical range of 1.0–1.3 for x, the fractal backbone dimension, α was estimated from Eq. 6 and is presented in Table 1. It is shown that α varies between 0.40 and 0.52 revealing that the elasticity of the pre-sheared suspensions stems from inter- and intra-floc links between nanotubes (Wu and Morbidelli 2001).

The effect of temperature

To investigate the effect of temperature on the suspensions microstructure, the variation of the limit for the linear viscoelastic region as well as the linear viscoelastic results at different concentrations was verified when the temperature was varied from 15°C to 45°C. It should be noted that although the range of temperatures used was limited, its influence on the LVE results was significant. To ensure the sample had a uniform temperature after being loaded into the rheometer, it was kept in quiescent conditions for 10 min before running any experiments.

Initially, the maximum strain for the limit of linearity was determined for each concentration at different temperatures. The results are summarized in Table 2. It can be observed that for each suspension, γ_c decreased with temperature revealing the formation of a more fragile structure as the temperature increased. However, the influence of temperature on γ_c was more pronounced at lower concentrations.

The effect of temperature on the LVE properties was determined for the suspensions as well as the neat epoxy. The complex viscosity, storage, and loss moduli of the suspensions decreased with temperature as expected. However, to eliminate the influence of temperature on the viscosity of the matrix, the results were reduced using the norm of the complex modulus of the neat epoxy at each temperature. The reduced storage and loss moduli for a 2 wt.% suspension reported in Fig. 9 show a drastic increase with temperature; however, this effect is more pronounced on the reduced storage modulus. A similar behavior was observed at other concentrations revealing the effect of increasing interaction between CNTs with temperature on the rheology of the suspensions.

Abbasi et al. (2009) observed that the reduced complex viscosity of polycarbonate–MWCNT nanocomposites increased with temperature revealing more inter-particle interactions, which is also in agreement

Table 1 Exponents from the scaling behavior of the LVE properties and fractal dimension as a function of pre-shear rate

$\dot{\gamma}_i$ (s^{-1})	γ_1	n	d_f	m	α
0.100	3.00 ± 0.08	0.69 ± 0.27	2.13 ± 0.14	0.38 ± 0.04	0.47–0.52
1.00	3.42 ± 0.14	0.96 ± 0.28	2.19 ± 0.09	0.36 ± 0.03	0.41–0.46
10.0	4.10 ± 0.08	1.10 ± 0.12	2.33 ± 0.02	0.37 ± 0.01	0.42–0.48
100	4.11 ± 0.33	1.18 ± 0.02	2.31 ± 0.15	0.36 ± 0.01	0.40–0.45

Table 2 Variations of γ_c (%) with temperature at various concentrations

c (wt.%)	$T = 15°C$	$T = 25°C$	$T = 35°C$	$T = 45°C$
2	2.41	1.94	1.46	1.01
3	1.72	1.26	0.96	0.78
5	0.67	0.64	0.48	0.60
6	0.79	0.58	0.38	0.43

with our results. However, in contrast to the results of this work, they reported increases of γ_c and cohesive energy ($E_c = 0.5\gamma_c^2 G_0'$, the work required to break-up the elastic structure) with temperature, revealing the formation of stronger network. From a structural point of view, they argued that the increase in temperature results in the breakdown of CNT bundles to individual nanotubes; thus the effective aspect ratio of nanotubes increased, which resulted in lower percolation thresholds and higher intrinsic viscosities at higher temperatures.

The time–temperature superposition was verified for the suspensions in the temperature range of 15°C to 45°C using the reduced storage modulus data. Since the neat epoxy is Newtonian, the reduced storage modulus corresponds to the contribution of CNTs. The results are reported in Fig. 10. The angular frequency was multiplied by a shift factor, a_T taken the reference temperature at 15°C. The y-axis for the 6 wt.% suspension was multiplied by a factor 10 to avoid overcrowding with the one for the 5 wt.%. This figure shows that the time–temperature superposition principle, which is valid for pure polymers, is also valid for the CNT suspensions. This is in accordance with our previous observation (Khalkhal et al. 2011) for collapsing the steady-shear viscosity data of a CNT suspension on a master curve for a similar temperature range. Note from Fig. 10a,

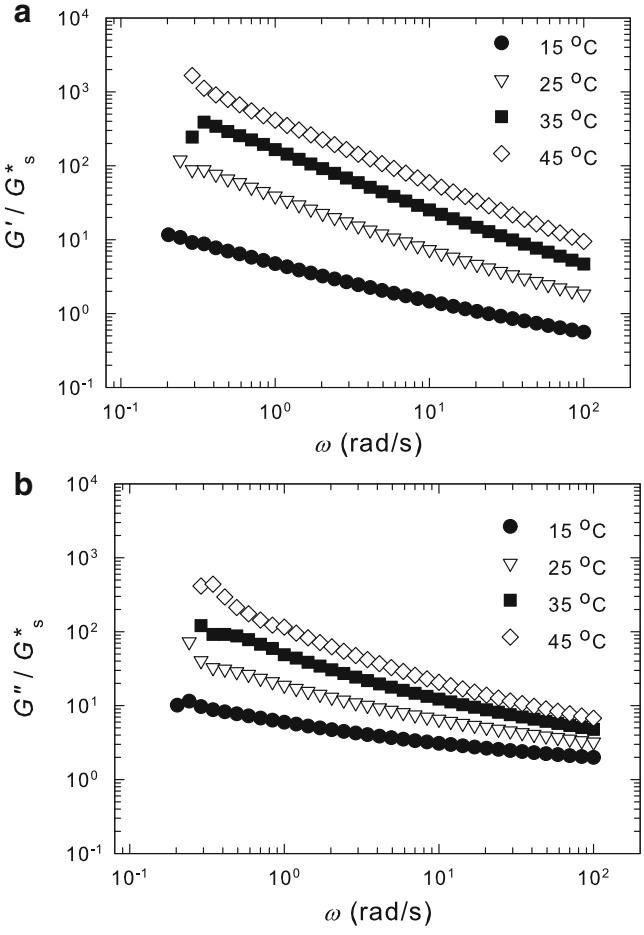

Fig. 9 The effect of temperature on the frequency sweep results of a 2 wt.% MWCNT–epoxy suspension **a** reduced storage modulus and **b** reduced loss modulus. G_s^* is the norm of the complex modulus of the neat epoxy

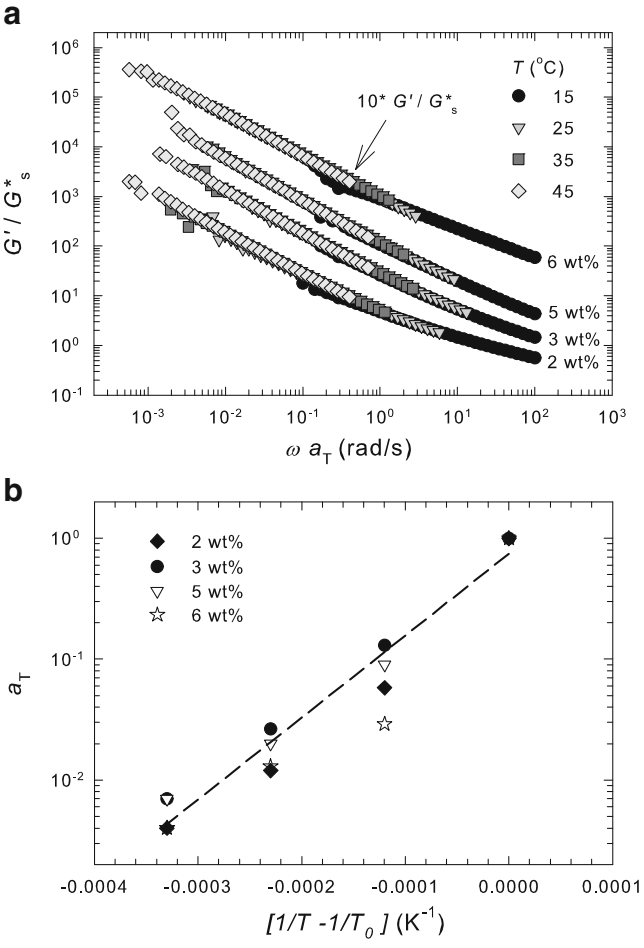

Fig. 10 **a** Time–temperature superposition for reduced storage modulus of MWCNT suspensions in epoxy; G_s^* is the norm of the complex modulus of the neat epoxy, **b** variation of the shift factor a_T with absolute temperature at various concentrations

Table 3 Variations of the scaling exponents with temperature

T(°C)	γ_1	n	d_f	m	α
15	2.740 ± 0.167	1.167 ± 0.274	1.72 ± 0.09	0.29 ± 0.04	0.17–0.25
25	3.442 ± 0.058	1.131 ± 0.084	2.13 ± 0.01	0.34 ± 0.01	0.34–0.40
35	2.922 ± 0.391	1.223 ± 0.051	1.77 ± 0.25	0.29 ± 0.02	0.19–0.26
45	2.868 ± 0.060	0.707 ± 0.158	2.07 ± 0.04	0.38 ± 0.02	0.45–0.50

the angular frequency is extended by more than two decades, down to 10^{-3} rad/s compared to 10^{-1} rad/s in Fig. 9, which was practically inaccessible at high concentrations. Moreover, the reduced storage modulus for the 5 wt.% suspension is almost a decade larger than the one for the 3 wt.% suspension (and similarly, the reduced storage modulus of the 3 wt.% suspension was almost a decade larger than the one for the 2 wt.%) at similar angular frequencies that can be associated to more inter-particle interactions due to the increase in concentration. However, the reduced modulus for the 5 and 6 wt.% suspensions are almost similar. Figure 10b reports the shift factor a_T, as a function of $1/T$. From this figure, there is only a small variation of a_T with concentration, which shows that the increase of the CNT interactions with temperature is almost independent of concentration. a_T is shown to scale exponentially with $1/T$ (straight line in Fig. 10b), revealing the fact that the time–temperature superposition is accounted for by an Arrhenius correlation:

$$a_T = \exp\left[\frac{E_a}{R}\left(\frac{1}{T} - \frac{1}{T_0}\right)\right], \tag{16}$$

where E_a is the activation energy, R is the gas constants (8.314 J/K), and T_0 (K) is the reference temperature which is considered to be 15°C (288 K). Using Eq. 16, an average E_a is calculated from curve fitting in Fig. 10b, which is equal to 129.7 kJ ($R^2 = 0.979$). This is the energy required for the molecules to move against the internal flow barriers caused by friction between the neighboring molecules.

For non pre-sheared suspensions, the scaling behavior of the low angular frequency storage modulus G'_0 at 1 rad/s and the maximum strain for the limit of linearity γ_c was verified at different temperatures and the power-law exponents γ_1 (from $G'_0 \sim \phi_v^{\gamma_1}$) with $R^2 =$ 0.930 to 0.999 and n with $R^2 = 0.923$ to 0.997 were obtained and reported in Table 3. From these exponents the fractal dimension d_f was calculated as a function of temperature using Eqs. 5–7. The results show the variations of d_f with temperature; however, the variations do not show a clear trend and the differences in the fractal dimensions remain in the range of the experimental error. Moreover, the exponent m varies from 0.29 to 0.38 and remains within the limit of soft and rigid aggregates. α was also calculated to be within [0,1] revealing that the suspensions elasticity originates from both inter- and intra-floc links.

From the results reported on the effect of temperature, one can conclude that the inter-particle interactions increase with temperature as shown in Fig. 9; however it is impossible to clarify whether the superstructure becomes more open or compact with temperature. This could be due to the limited temperature range of this system (only 30°C temperature difference) although the linear viscoelastic properties of the suspensions were significantly influenced by temperature in this range.

Conclusion

The scaling behavior of linear viscoelastic properties of MWCNT–epoxy suspensions was investigated with and without pre-shearing history. Initially, the suspensions fractal dimension d_f was approximated to be about 2.15, characteristic of slowly flocculating suspensions where flocs gradually penetrate one another to some extent after collision. In addition, the elasticity of the network structure of the suspensions was shown to originate from the contribution of inter- and intra-floc links between nanotubes.

From the master curve of the steady-shear results normalized with the low angular frequency storage modulus of the pre-sheared suspensions, G'_∞, it was concluded that G'_∞ that varies with the pre-shear rate and concentration can account for most of the structural changes during flow and thus is a suitable parameter for characterizing the structure of CNT suspensions. The power-law exponents of G'_∞ and γ_c demonstrated a significant increase with applied pre-shear rate; however, the resulting d_f and so the superstructure of the network of the suspensions exhibited only a small variation with flow history that was related to the initially dense structure of the suspensions before pre-shearing ($d_f \sim 2.15$). As one of the applications of CNT suspensions is in preparing conductive nano-composites, it is important to preserve the network structure of the suspensions during processing.

The power-law exponent m revealing the variation of the radius of gyration of the aggregates with the applied shear rate $\left(\xi \sim \dot{\gamma}^{-m}\right)$ was found to be in the

range of 0.36–0.38 and in the limit for m_{rigid} and m_{soft} obtained theoretically by Potanin (1993) and similar to the experimental values obtained by Sonntag and Russel (1986, 1987). This shows that the interaction potential of nanotubes is a combination of central and non-central components.

Finally, the effect of temperature on the scaling behavior of the suspensions was verified with no pre-shear history except for the sample loading into the instrument. It was observed that the reduced storage and loss moduli of the suspensions increased with temperature, suggesting more interactions between CNTs. Moreover, the time–temperature superposition principle was verified for the CNT suspensions and the shift factor was found to obey an Arrhenius equation. However, the estimated fractal dimension had large errors that made it difficult to identify whether the superstructure of the suspensions change as influenced by temperature.

Acknowledgements We are thankful to Dr. Daniel Therriault for providing access to the three roll mill at the composite lab in the mechanical engineering department of Ecole Polytechnique. Funding from Natural Sciences and Engineering Research Council of Canada (NSERC) and Consortium for Research and Innovation in Aerospace in Quebec (CRIAQ) is gratefully acknowledged.

References

Abbasi S, Carreau PJ, Derdouri A, Moan M (2009) Rheological properties and percolation in suspensions of multiwalled carbon nanotubes in polycarbonate. Rheol Acta 48(9):943–959

Buscall R, McGowan IJ, Mills PDA, Stewart RF, Sutton D, White LR, Yates GE (1987) Rheology of strongly-flocculated suspensions. J Non-Newton Fluid Mech 24(2):183–202

Chatterjee T, Krishnamoorti R (2007) Dynamic consequences of the fractal network of nanotube-poly(ethylene oxide) nanocomposites. Phys Rev E Stat Nonlinear Soft Matter Phys 75(5):050403

Chen M, Russel WB (1991) Characteristics of flocculated silica dispersions. J Colloid Interface Sci 141(2):564–577

Chow MK, Zukoski CF (1995) Nonequilibrium behavior of dense suspensions of uniform particles: volume fraction and size dependence or rheology and microstructure. J Rheol 39(1):33–59

de Gennes PG (1979) Scaling concepts of polymer physics. Cornell University Press, Ithaca

Fagan ME, Zukoski CF (1997) Rheology of charge stabilized silica suspensions. J Rheol 41(2):373–397

Fan Z, Advani SG (2007) Rheology of multiwall carbon nanotube suspensions. J Rheol 51(4):585–604

Fry D, Langhorst B, Kim H, Grulke E, Wang H, Hobbie EK (2005) Anisotropy of sheared carbon-nanotube suspensions. Phys Rev Lett 95(3):038304

Fry D, Langhorst B, Wang H, Becker ML, Bauer BJ, Grulke EA, Hobbie EK (2006) Rheo-optical studies of carbon nanotube suspensions. J Chem Phys 124(5):054703

Hobbie EK, Fry DJ (2006) Nonequilibrium phase diagram of sticky nanotube suspensions. Phys Rev Lett 97(3):036101

Hobbie EK, Fry DJ (2007) Rheology of concentrated carbon nanotube suspensions. J Chem Phys 126(12):124907

Hobbie EK, Wang H, Kim H, Han CC, Grulke EA, Obrzut J (2003a) Optical measurements of structure and orientation in sheared carbon-nanotube suspensions. Rev Sci Instrum 74(3 I):1244–1250

Hobbie EK, Wang H, Kim H, Lin-Gibson S, Grulke EA (2003b) Orientation of carbon nanotubes in a sheared polymer melt. Phys Fluids 15(5):1196–1202

Huang YY, Ahir SV, Terentjev EM (2006) Dispersion rheology of carbon nanotubes in a polymer matrix. Phys Rev B: Condens Matter 73(12):125422

Khalkhal F, Carreau PJ, Ausias G (2011) Effect of flow history on linear viscoelastic properties of MWCNT suspensions in an epoxy. J Rheol 55(1):153–175

Larson RG (1999) The structure and rheology of complex fluids. Oxford University Press, New York

Lin-Gibson S, Pathak JA, Grulke EA, Wang H, Hobbie EK (2004) Elastic flow instability in nanotube suspensions. Phys Rev Lett 92(4):48302

Mobuchon C, Carreau PJ, Heuzey MC (2009) Structural analysis of non-aqueous layered silicate suspensions subjected to shear flow. J Rheol 53(5):1025–1048

Potanin AA (1991) On the mechanism of aggregation in the shear flow of suspensions. J Colloid Interface Sci 145(1):140–157

Potanin AA (1993) On the computer simulation of deformation and breakup of colloidal aggregates in shear flow. J Colloid Interface Sci 157:399–410

Potanin AA, De Rooij R, Van den Ende D, Mellema J (1995) Microrheological modeling of weakly aggregated dispersions. J Chem Phys 102(14):5845–5853

Pujari S, Rahatekar SS, Gilman JW, Koziol KK, Windle AH, Burghardt WR (2009) Orientation dynamics in multiwalled carbon nanotube dispersions under shear flow. J Chem Phys 130(21):214903

Rahatekar SS, Koziol KKK, Butler SA, Elliott JA, Shaffer MSP, Mackley MR, Windle AH (2006) Optical microstructure and viscosity enhancement for an epoxy resin matrix containing multiwall carbon nanotubes. J Rheol 50(5):599–610

Shih W-H, Shih WY, Seong-Il K, Jun L, Alsay IA (1990) Scaling behavior of the elastic properties of colloidal gels. Phys Rev A 42(8):4772–4779

Song YS, Youn JR (2005) Influence of dispersion states of carbon nanotubes on physical properties of epoxy nanocomposites. Carbon 43(7):1378–1385

Sonntag RC, Russel WB (1986) Structure and breakup of flocs subjected to fluid stresses: I. Shear experiments. J Colloid Interface Sci 113(2):399–413

Sonntag RC, Russel WB (1987) Structure and breakup of flocs subjected to fluid stresses: II. Theory. J Colloid Interface Sci 115(2):378–389

Switzer LH III, Klingenberg DJ (2003) Rheology of sheared flexible fiber suspensions via fiber-level simulations. J Rheol 47(3):759–778

Wu H, Morbidelli M (2001) A model relating structure of colloidal gels to their elastic properties. Langmuir 17(4):1030–1036

Wu D, Wu L, Zhou W, Sun Y, Zhang M (2009) Relations between the aspect ratio of carbon nanotubes and the formation of percolation networks in biodegradable polylactide/carbon nanotube composites. J Polym Sci Part B Polym Phys 48(4):479–489